Enhanced Efficacy of Pluronic Copolymer Micelle Encapsulated SCR7 against Cancer Cell Proliferation[a]

Franklin John, Jinu George,* Supriya V. Vartak, Mrinal Srivastava, P. A. Hassan, V. K. Aswal, Subhas. S. Karki, Sathees C. Raghavan

5,6-Bis(benzylideneamino)-2-mercaptopyrimidin-4-ol (SCR7) is a new anti cancer molecule having capability to selectively inhibit non-homologous end joining (NHEJ), one of the DNA double strand break (DSB) repair pathways inside the cells. In spite of the promising potential as an anticancer agent, hydrophobicity of SCR7 decreases its bioavailability. Herein the entrapment of SCR7 in Pluronic copolymer is reported. The size of the aggregates was determined by transmission electron microscopy (TEM) and dynamic light scattering (DLS) which yields an average diameter of 23 nm. SCR7 encapsulated micelles (ES) were also characterized by small-angle neutron scattering (SANS). Evaluation of its biological properties by using a variety of techniques, including Trypan blue, MTT and Live-dead cell assays, reveal that encapsulated SCR7 can induce cytotoxicity in cancer cell lines, being more effective in breast cancer cell line. Encapsulated SCR7 treatment resulted in accumulation of DNA breaks within the cells, resulting in cell cycle arrest at G1 phase and activation of apoptosis. More importantly, we found ≈ 5 fold increase in cell death, when encapsulated SCR7 was used in comparison with SCR7 alone.

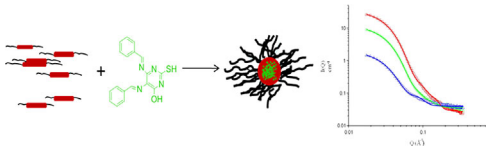

Dr. F. John, Dr. J. George
Biotechnology Laboratory, Department of Chemistry, Sacred Heart College, Kochi 682 013, India
E-mail: jinujacobv@gmail.com
S. V. Vartak, Dr. M. Srivastava, Dr. S. C. Raghavan
Department of Biochemistry, Indian Institute of Science, Bangalore 560 012, India
Dr. P. A. Hassan
Chemistry Division, Bhabha Atomic Research Centre, Mumbai 400 085, India
Dr. V. K. Aswal
Solid State Physics Division, Bhabha Atomic Research Centre, Mumbai 400 085, India
Dr. S. S. Karki
Department of Pharmaceutical Chemistry, KLE University, Bangalore 560 010, India

[a]**Supporting Information** is available online from the Wiley Online Library or from the author.

1. Introduction

Cancer is one of the most common diseases that are manifested in about a third of the population in some form or other.[1] Cancer follows a number of mutagenic processes which allow cancer cells to acquire properties of unlimited proliferation potential, self-sufficiency in growth signals and resistance to both anti-proliferative and apoptotic cues which would, otherwise, contain their growth.[2,3] Cancer drug targeting is challenged by problems like multi-drug resistance (MDR). [4] MDR imparts on cancer cells the ability to pump out toxic anti-cancer agents before they can kill the cells. Active efflux, enzymatic modification and modification of target receptor or enzyme are the three main route causes for drug resistance. There are two general classes of resistance to anti-cancer drugs: those that impair delivery

DOI: 10.1002/mabi.201400480

of anti-cancer drugs to tumor cells, and those that arise in the cancer cell itself due to genetic and epigenetic alterations that affect drug sensitivity. Impaired drug delivery can result from poor absorption of orally administered drugs, increased drug metabolism or increased excretion, resulting in lower levels of drug in the blood and reduced diffusion of drugs from the blood into the tumor.[5,6]

Therapeutic approach against cancer is widely classified into two groups: cytotoxic therapies and molecular targeted drugs. Examples of traditional cytotoxic therapies include radiation and chemotherapeutic compounds such as platinum-based drugs.[7–10] Among the different DNA damages, DNA double strand breaks (DSBs) are considered as the most lethal as it affects the integrity and continuity of the genome.[11–14] Inappropriate repair of DSBs could result in deletions, inversions, duplications and chromosomal translocations.[15–18] Non-homologous DNA endjoining (NHEJ) is one of the major DNA DSB repair pathways.[19] Recently, a novel inhibitor of NHEJ, 5,6-bis(benzylideneamino)-2-mercaptopyrimidin-4-ol (SCR7, Figure 1) has been reported, which acts by targeting DNA binding domain of Ligase IV.[20] Using various biochemical and biophysical assays, it was established that SCR7 can target NHEJ in both in vitro and ex vivo. Inhibition of NHEJ by SCR7 in cancer cells results in the accumulation of unrepaired DNA DSBs, which in turn activated p53 mediated pathway of apoptosis. SCR7 impeded tumor progression in different tumor models. More importantly, when SCR7 was co-administered along with radiation and certain chemotherapeutic agents, it significantly enhanced their antitumor effects. Despite promising results of SCR7 as a good anticancer agent, it showed high concentration of 50% inhibition (IC_{50}), which could be attributed to its high hydrophobicity.

Although SCR7 has shown promising results as a potential anticancer drug, its limited solubility in water may lead to poor bioavailability and demands the search for novel drug delivery systems. Traditional methods to improve the bioavailability of poorly soluble drugs include encapsulating them in nanosized carriers such as liposomes,[21] emulsions, polymer micelles,[22] niosomes,[23] lipid particles, etc. Poly(ethylene glycol)[24] (PEG) based block copolymers have the distinct advantage, as compared to other delivery systems, due to its ability to encapsulate large amounts of drug, having stealth nature and well defined size with narrow polydispersity. Biodegradable and non-biodegradable polymers have been used for the past few decades for encapsulating various anticancer drugs. Encapsulation of drug within a micelle increases the drug's effective solubility in the bloodstream, allowing smaller doses to be delivered with the same effect.[25] Polymer-conjugated drugs[26,27] generally exhibit prolonged half-life, higher stability, water solubility, lower immunogenicity and antigenicity and often also specific targeting to tissues or cells. Mechanism of the subsequent drug delivery, and the role of encapsulating polymer in preventing the biological degradation prior to the drug release is well established.[28–30] The core shell structure of polymeric micelles aid the system to incorporate poorly soluble drugs and protect them from inactivation in biological media. The particle size distribution in these systems is rather narrow with a size range typically less than 30 nm and therefore, these systems exhibit many advantages such as targeting ability, long circulation and easy production on effective delivery of drugs. Copolymeric micelles were extensively developed for drug delivery of anticancer drugs.[31–33] One representative of such materials is Pluronic block copolymers that are amphiphilic synthetic polymers containing hydrophilic poly(ethylene oxide) (PEO) blocks and hydrophobic poly(propylene oxide) (PPO) blocks arranged in triblock structure: PEO-PPO-PEO.[34] One of the advantages of working with block copolymers is the versatility in precisely controlling nanostructure.[35–40] Because of their lower critical solution temperature (LCST), which is around body temperature they have been widely used in the development of controlled drug delivery systems based on sol-gel phase conversion at the body temperature. Controlled release systems are known to enhance effectiveness of drug therapy.[41] In order to increase the bioavailability of SCR7 and to reiterate the use of amphiphilic copolymer as a better release system, we report the preparation of SCR7 encapsulated with Pluronic P123 copolymer (ES), its microstructure characterization in micellar form and evaluation of its biological activity.

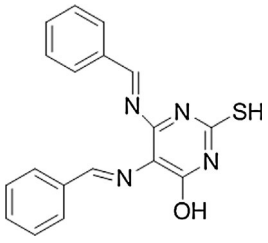

Figure 1. Structure of SCR7.

2. Experimental Section

2.1. Materials

Pluronic P123 and D_2O were purchased from Aldrich (Bangalore, India). All the salts and solvents used in the study were purchased from Merck (Mumbai, India), Sigma Chemical Co. (St. Louis, MO),

Amresco (USA) and SRL (India). All other reagents and buffer solution components were analytical grade preparations. Distilled and deionized water was used in all experiments.

2.2. Methods

2.2.1. Preparation of SCR7-loaded Polymeric Micelles and In Vitro Drug Release

SCR7 was synthesized as described earlier.[20] SCR7 loaded micelle was prepared by thin-film hydration method.[34] Eight mg of SCR7 and 320 mg of Pluronic block copolymer P123 were dissolved in 10 ml acetonitrile in a round-bottom flask. The solvent was evaporated by rotary evaporation at 50 °C for about 1 h to obtain a solid SCR7-P123 matrix. Residual acetonitrile remaining in the film was removed under vacuum overnight at room temperature. The resultant thin film was hydrated with water. The mixture was stirred at 700 rpm for 30 min to obtain a micelle solution, which was then filtrated through 0.2 μm filter membrane to remove the unincorporated drug aggregates, followed by lyophilization. The in vitro release behavior of SCR7 from SCR7 encapsulated Pluronics was monitored in phosphate-buffered saline (PBS; pH 7.4) with 0.2% Tween-80 by dialysis method.[42] One ml free SCR7 solution or 1 ml SCR7 loaded micelles (containing 0.1 mg SCR7) was kept in dialysis bag (molecular weight cut-off (MWCO): 5000 Da) and the bag was submerged fully into 40 mL of PBS (pH 7.4) with 0.2% Tween-80 at 37 °C. At appropriate time intervals (0, 1, 4, 8, 12, 24, 48, 72, and 92 h), 0.5 mL aliquots were withdrawn and replaced with same amount of fresh medium. The content of SCR7 was determined by Reverse Phase High Performance Liquid Chromatography (RP-HPLC) (LC 2010 C HT Shimadzu, Kyoto, Japan) assay after solubilization in acetonitrile. An isocratic flow of 65:35 (v/v) with a degassed mixture of acetonitrile/water as mobile phase and reverse phase column (Kintex 5 u C18, 250 mm × 4.6 mm, Phenomenex, California, USA) was used. The flow rate was set at 1.0 $mL \cdot min^{-1}$ and the samples were monitored by UV absorption at 227 nm. The retention time was around 5.1 min. The eluent was quantified by comparing the peak areas with standard curve. The drug-loading coefficient (DL) and encapsulation ratio (ER) were determined by the following equations:[43]

$$DL\% = \frac{\text{weight of the drug in micelles}}{\text{weight of the feeding polymer and drug}} \times 100\% \quad (1)$$

$$ER\% = \frac{\text{weight of the feeding polymer and drug}}{\text{weight of the feeding drug}} \times 100\% \quad (2)$$

2.2.2. Characterization of SCR7-loaded Polymeric Micelles

Fluorescence emissions were recorded on F-2500 fluorescence spectrometer (Hitachi, Japan). Shimadzu (UV-2450) UV-visible double beam spectrophotometer with matched pair of stoppered fused silica cells of 1 cm optical path length was used for UV spectroscopic measurements. Fourier transformed (FT) IR measurements were obtained using SHIMADZU 8400 FT IR spectrometer. ^{1}H NMR spectra was recorded on a Varian 400 MHz spectrometer (Varian, Palo Alto, CA, USA) in deuterated dimethyl sulfoxide (DMSO-d6), chloroform ($CDCl_3$) and water (D_2O) at room temperature. The mass spectrometric analysis was carried out by direct infusion in Xevo G2 (Waters, Milford, MA 01757, USA) Quadrapole-Time-of-Flight (Q-TOF) Mass spectrometer. Q-TOF mass spectrometers combine the high performance time-of-flight analysis in both mass spectrometry (MS) and tandem MS (MS/MS) modes, with the widely used technique of electrospray ionization (ESI). The single and tandem mass spectra are obtained in the TOF analyzer, product ion spectra are recorded with the same high resolution, mass accuracy and even mass calibration as in single MS mode. One of the most useful features of TOF spectra for structural identification is very high mass accuracy, in the ppm range.[44] Transmission electron microscopy (TEM) images were obtained on an electron microscopy Igor 1200EX, operating at 80 kV of an accelerating voltage. Freshly prepared samples were prepared by dropping 5 μL aliquots of Pluronic micelle solution (H_2O) onto a TEM grid (400-mesh copper grid coated with carbon). After a few minutes, remaining solution was blotted off with a filter paper and images were collected. The size distribution of the micelles was measured by Dynamic Light Scattering (DLS) using a Malvern 4800 Autosizer employing 7132 digital correlator. The instrument is equipped with a 300 mW diode pumped solid state laser ($\lambda = 532$ nm) with a vertically polarized light and the measurements were carried out at a scattering angle of 130°. The apparent diffusion coefficients of the micelles are obtained from the normalized time correlation function of the scattered electric field, $g^{(1)}(\tau)$, using the cumulants analysis which follows

$$\ln[g^1(\tau)] = \ln\beta - \Gamma\tau + \frac{\mu_2\tau^2}{2} \quad (3)$$

where Γ is the mean relaxation rate given by $\Gamma = Dq^2$ (D being the translational diffusion coefficient and q, the wave vector transfer), μ_2 is the variance in the relaxation rate distribution and β is the baseline. The hydrodynamic diameter (R_d) is obtained from the translational diffusion coefficient using the Stokes-Einstein relationship

$$R_d = kT/(3\pi\eta D_h) \quad (4)$$

where k is the Boltzmann constant, η is the solvent viscosity and T is the absolute temperature. Small-angle neutron scattering (SANS) experiments were carried out using the SANS diffractometer at Dhruva Reactor, Bhabha Atomic Research Centre, Trombay, India. The diffractometer makes use of a beryllium oxide filtered beam of mean wavelength (λ) of 5.2 Å. The angular distribution of the scattered neutrons was recorded using a one- dimensional position sensitive detector (PSD). The accessible wave vector transfer [$q = 4\pi\sin\theta/\lambda$, where 2θ is the scattering angle and range of the diffractometer is 0.02–0.32 $Å^{-1}$]. The PSD allows simultaneous recording of data over the full q range. The samples were held in a quartz sample holder of 0.5 cm thickness. All the measurements were carried out at room temperature. The measured SANS data

were corrected and normalized to a cross sectional unit, using standard procedures.

2.2.3. Thin Layer Chromatography (TLC) and Thermal Analysis

TLC method was adopted to study the physical interaction of SCR7 and P123. A mixture of 10% methanol in chloroform was used as mobile phase and silica gel G was used as the stationary phase. The spots were detected under UV light and stained using alkaline $KMnO_4$ solution and R_f values were determined.[45] Thermal stability of the drug polymer conjugates were analyzed by thermogravimetric analysis (TGA) and differential scanning calorimetry (DSC). TGA was carried out using TGA-Pyres-6TGA (Perkin Elmer, UK), by heating from 40 °C to 730 °C at a heating rate of 10 K min^{-1} under N_2 flow. DSC experiments were carried out in a DSC Q100 V7.3 Build 249 (DSC standard cell) at a heating rate of 20 K min^{-1} in the range of 40 °C to 300 °C under the steady flow of N_2.

2.2.4. Evaluation of Cytotoxicity in Cancer Cell Lines

Nalm6 (Leukemia cell line) and MCF7 (breast cancer cell line) cells were seeded at the density of 20 000 cells/well. After 24 h of treatment, cells were treated with increasing concentrations of encapsulated form of SCR7. Equivalent concentration of encapsulation matrix alone was used as the control. Following 48 h of treatment, cytotoxicity was assessed by Trypan blue dye exclusion and 3-(4,5-dimethylthiazol-2-yl)-2,5-diphenyltetrazolium bromide (MTT) assays.[46,47] Each experiment was independently repeated minimum of 4 times. Graph was plotted (Graphpad Prism Version 5) and error bars are indicated.

2.2.5. Live-dead Cell Assay

Nalm6 and MCF7 cells were seeded and treated as described above. After 48 h of treatment, cells were harvested, washed and subjected to live-dead cell assay as described.[48] Briefly, cells were stained with 0.5 $\mu g \cdot ml^{-1}$ of ethidium bromide and acquired using fluorescence-activated cell sorting (FACS) verse from Becton Dickinson (BD). Data was analyzed by WinMDI and plotted as density plot.

2.2.6. Cell Cycle Analysis

In order to investigate the effect of encapsulation of SCR7 on cell progression, Nalm6 and MCF7 cells were seeded and treated (0, 0.05, 0.1, 0.2 and 0.5 $mg \cdot ml^{-1}$) as described earlier.[49,50] After 48 h of treatment, cells were harvested, washed and stored at –20 °C (4 h). Followed by fixing, cells were spun, washed and treated overnight with 50 $\mu g \cdot ml^{-1}$ RNase A. Cells were stained with 0.1 $\mu g \cdot ml^{-1}$ of propidium iodide (PI) and acquired using BD FACS verse. Data was analyzed by WinMDI and plotted as histogram. Distribution of percentage of cells in different cell cycle phases was plotted (Graphpad Prism Version 5).

2.2.7. Annexin V-FITC/PI Staining

Annexin V-fluorescein isothiocyanate (FITC)/PI staining was performed as recommended in manufacture's protocol. Following treatment with encapsulated form of SCR7 (0, 0.1, 0.2 and 0.5 $mg \cdot ml^{-1}$) for 48 h, cells were harvested, washed and stained with Annexin-FITC for 1 h. Cells were stained with PI for 15 min, washed and suspended in 1× PBS. Cells were acquired by BD FACS verse and plotted density plot with the help of WinMDI as described earlier.[51]

2.2.8. Immunocytochemistry

Nalm6 cells (0.25×10^5) were cultured in 6 well plates for 24 h, followed by treatment with either SCR7 (100×10^{-6} M) or ES (0.4 $mg \cdot ml^{-1}$). DMSO-treated cells were used as control. After 24 h treatment, cells were harvested, fixed (4% paraformaldehyde for 10 min) and processed for immunocytochemistry.[20] Briefly, following fixing, cells were permeabilized (PBS containing 0.1% Triton X-100 for 5 min) and blocked (PBST containing 0.1% BSA and 10% foetal bovine serum (FBS) for 1 h). Cells were incubated with anti-γ-H2AX antibody (1:500; Millipore) overnight at 4 °C, washed with PBST and incubated with corresponding biotinylated secondary antibody (1:200) for 2 h. Cells were then washed, incubated with streptavidin-FITC (1:1000) for 20 min, stained with PI, and mounted using diazobicyclo[2.2.2]octane (DABCO). Images of cells with γ-H2AX foci were taken using Zeiss Laser Confocal microscopy (Germany) or Olympus DSU fluorescent microscope (Japan).

2.2.9. Comet Assay

Following treatment with either SCR7 (100×10^{-6} M), ES (0.4 $mg \cdot ml^{-1}$) or DMSO (control), Nalm6 cells (0.25×10^5) were cultured in 6 well plates for 24 h. After treatment, cells were harvested and processed for Comet assay as described.[52] Briefly, cells were washed with PBS, mixed with 1% low melting agarose and coated onto glass slides. Cells were then subjected to lysis in an alkaline buffer condition, followed by electrophoresis. Electrophoresis of samples was carried out (0.6 $V \cdot cm^{-1}$ for 25 min), slides were neutralized, stained with PI and visualized. About 20 cells were imaged per sample for each experiment, scored for comets using CometScore software and analyzed for % DNA in tail, tail moment and Olive moment.

3. Results and Discussion

3.1. In Vitro Release Studies

The DL% and ER% were determined by Equation (1) and (2) as $1.39 \pm 0.04\%$ and $95 \pm 3.91\%$, respectively for the composition of 1:40 of SCR7:P123. Even though drug release is expected to be pH dependent,[53] we attempted only the release at physiological pH 7.4. Pluronic copolymer showed good encapsulation ability for SCR7, which consists of aromatic and heterocyclic systems. In vitro release profile (Figure SI, Supporting Information) indicated that nearly 80% of SCR7 was released within 4 d.

3.2. Analytical Characterization

3.2.1. Fluorescence and UV-Vis Spectra

The fluorescence emission spectra of SCR7 showed a blue shift upon encapsulation with P123 copolymer in DMSO as shown in Figure 2a. SCR7 in DMSO exhibits an emission peak at ≈474 nm, while SCR7 in the presence of P123 show a maximum at ≈442 nm in the same solvent (DMSO due to the high solubility of SCR7). The shift in the λ_{max} of fluorescence spectrum is an indication of interaction between SCR7 and the copolymer P123. Such shift in the fluorescence emission is reported for doxorubicin encapsulated with chitosan nano particles and curcumin casein micelles.[54,55] The blue-shift in the fluorescence is likely due to the changes in the microenvironment of SCR7 within the hydrophobic core of P123.[56]

UV-Vis absorption spectra of SCR7-P123 in water (Figure 2b) showed that addition of P123 enhances the solubility of SCR7. The hydrophobic PPO core of the copolymer effectively encapsulates the drug molecule and makes it dispersible the the aqueous layer. To reiterate the encapsulation and release of SCR7 from P123, the aqueous layer was extracted with chloroform (3 ×). The chloroform layer was dried with Na_2SO_4. The UV absorption spectra of the chloroform layer show maxima at 267 nm and 365 nm. The optical absorption spectrum of the chloroform layer is compared with SCR7 in pure water and SCR7 encapsulated P123 in water. This indicates the ability of P123 to encapsulate the drug and its release upon treatment with hydrophobic solvents like chloroform.

3.2.2. FT-IR, NMR and MS/MS Spectra

FT-IR spectra (Figure SII, Supporting Information) of SCR7 and SCR7 encapsulated with P123 showed evidence for drug encapsulation. The C–N stretching vibrations occur at 1094 cm^{-1}. The absorption occurring at 1367 cm^{-1} is due to C–H stretching vibrations, that at 1639 cm^{-1} is due to CN stretching vibration.[57] The absorptions at 1296 $cm^{-1}$and 1031.1 cm^{-1} are due to C–O stretching vibrations from the P123 matrix. The absorptions at 931 cm^{-1} and 851 cm^{-1} are arising from the aromatic ring of SCR7 and that at 2972 cm^{-1} corresponds to O-H group. There was no appreciable shift in the IR signal of SCR7 observed when it changes from free state to polymer bound state. It can also be concluded that there was no chemical interaction takes place between P123 and SCR7. The result confirmed the presence of SCR7 in the encapsulated formulation.

Successful incorporation of SCR7 in P123 and its release in different solvents were elucidated by ^{1}H NMR spectroscopy (Figure SIII, Supporting Information). In ^{1}H NMR spectrum of SCR7-P123 employing DMSO-d6 as solvent, characteristic aromatic signals from SCR7 at 7.1–7.5 ppm were observed. D_2O and $CDCl_3$ were also used as solvent. In all the spectra, the aromatic proton signals corresponding to SCR7 are seen with lower intensity compared with the Pluronic counterpart.

^{1}H signals from the hydrophobic part of the copolymer were seen in D_2O. However, the PPO segments in pluronic micelles are loosely bound and there is still mobility of the chains. It is expected that a broadening of the peak with association may occur, but the broadening is not large enough to mask the lines. It may be noted that pure SCR7 in D_2O does not show any appreciable signal due to poor solubility of the drug in water. However, the occurrence of aromatic proton signals in D_2O in the presence of P123 is an indication of encapsulation of the drug in the micelle. Different solvents were used to see whether there is any change in intensity of SCR7 signal due to difference in release property. Moreover, the signals in D_2O are broader

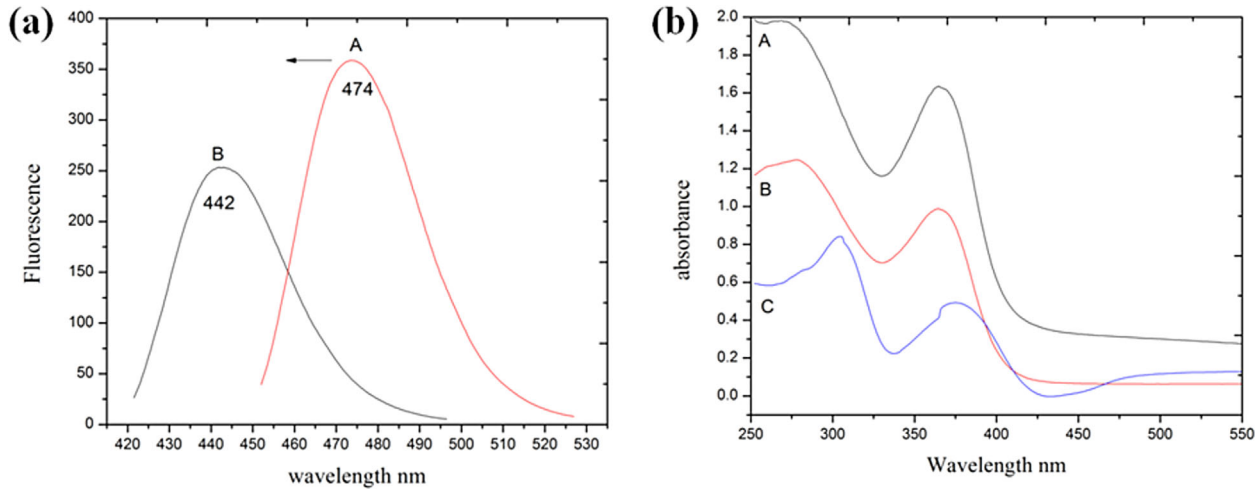

Figure 2. (a) (A) Fluorescence emission spectra of SCR7 in DMSO; (B) SCR7 loaded P123 in DMSO. (b) (A) UV absorption spectra of SCR7 loaded P123 in water; (B) chloroform extract (C) SCR7 alone in water.

than that in $CDCl_3$ or DMSO. This is due to the association of the drug in the polymer matrix which restricts the tumbling motion of drug molecules.

The TOF Mass spectra from Pluronic polymer P123 were acquired to investigate the mass distribution pattern from the drug encapsulated polymer matrix (Figure SIV, Supporting Information). The significant fragmented ion peaks from the PEO and PPO parts of the polymer are observed in the region of *m/z* ranging from 50 to 850. The peak at *m/z* 233.16 showed the strongest intensity in the low mass range from P123. The fragments from pure P123 were observed at *m/z* value of 59 from $[CH_3–CH_2–O–CH_2]^+$ which is in agreement with published data from a Pluronic polymer P104.[56] The fragmented mass distribution shows two series of the distributions derived from PPO component, $[(PO)_n + Na]^+$ and $[(PO)_n + O + Na]^+$ with "n" ranging from 7 to 20, where sodium participated in the ionization process as an ionization assisting agent. PEO fragment ion distributions were observed in the mass range over 400 *m/z*, $[(EO)_n + Na]^+$ and $[(EO)_n + O + Na]^+$ with "n" ranging from 9 to 31. The MS/MS spectrum clearly indicates the presence of entrapped SCR7 in polymeric micelle. The selected *m/z* value is 335.09 from the $[M + H]^+$ where M represents the molecular ion.

3.2.3. TEM, DLS and SANS

To ascertain the size distribution of SCR7 encapsulated micelles, TEM measurements were made on specimens dried over a carbon coated Cu grid. As seen from the TEM image (Figure 3), a few spherical micelle-like particles can be seen with typical size of the order of 20–30 nm. However, there are many large clumps observed which could be interpreted as aggregates or clusters of polymer-drug assemblies formed during evaporation of the solvent.

As micelle like aggregates are present in the presence of solvent (like water or D_2O), we explored in-situ measurements in the presence of solvent to assess SCR encapsulated micelles using DLS.

Figure 4a shows the autocorrelation function of SCR7-P123 assemblies in water at a concentration of 1.2% P123, at a drug-polymer ratio of 1:40. The solid line is a fit to the data using the method of cumulants (as described in the experimental section), which shows good agreement with the data, indicating monomodal distribution of aggregates. The best fit values of DLS data indicate the formation of micelles with hydrodynamic diameter of 22.8 nm with a polydispersity index (PDI) of 0.188. Particle size distribution extracted from the autocorrelation function using CONTIN algorithm (Figure 4b) again confirms the formation of micelles.

Further evidence for drug encapsulated micelles was obtained from SANS measurements. SANS can also provide

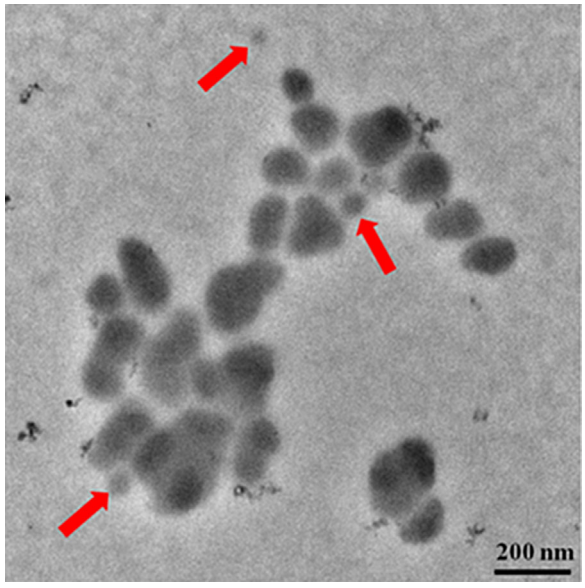

Figure 3. TEM image of SCR7 loaded P123.

evidence for interparticle interactions.[58] SANS experiments were widely used in the past to study associative interactions between pluronic triblock copolymers and drugs.[59] Figure 5 shows the SANS spectra of drug encapsulated polymer aggregates in D_2O at different drug-polymer ratios 1:2, 1:4 and 1:40. Among these three formulations, drug polymer ratio of 1:40 gives the best number of drugs per micelle as 35 for an encapsulation ratio of 95%. The SANS spectrum is similar to that of other reported dilute suspension of block copolymer assemblies.[60]

The SANS data were analyzed by assuming polydisperse core-shell spheres, of different scattering contrasts for the core and shell of the micelles with respect to the solvent. The scattering intensity as a function of the scattering vector (q) can be represented as

$$I_{coh}(q) = \frac{N_p}{V}\left[\frac{4\pi}{3}R_1{}^3(\rho_1 - \rho_2)\frac{3j_1(qR_1)}{qR_1} + \frac{4\pi}{3}R_2{}^3(\rho_2 - \rho_s)\frac{3j_1(qR_2)}{qR_2}\right]^2 \quad (5)$$

where j_1 is a spherical Bessel function given by

$$J_1(x) = \frac{\sin(x) - x \cdot \cos(x)}{x^2} \quad (6)$$

Here ρ_1, ρ_2 and ρ_s are the scattering length densities of the core, shell and solvent (water) respectively. R_1 is the core radius and R_2 is the shell radius given by R_{1+t}; t being the thickness. N_p is the number density of micelles and V is the volume of the micelle. A polydispersity in core radius, assuming a gaussian distribution with a PI of 0.2 is introduced in the fit.

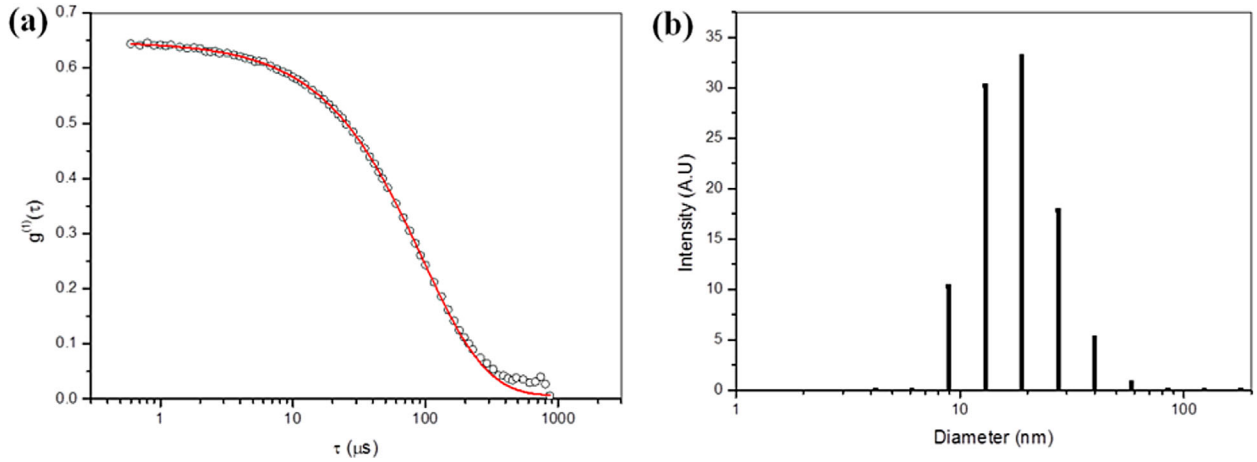

Figure 4. (a) Autocorrelation function of SCR7-P123 assemblies in water at a concentration of 1.2% P123, at a drug/polymer ratio of 1:40 (b) Particle size distribution extracted from the autocorrelation function using CONTIN algorithm.

Analysis of the SANS data indicates the formation of micelles with a core radius of 35 Å and a shell thickness of 46 Å. The variation in the micellar parameters with changes in the drug-polymer ratio is summarized in Table 1. With an increase in the drug to polymer ratio, the core radius increases while the shell thickness decreases. This is consistent with the expectation that the drug molecules are solublized in the core/palisade layer of the micelles with concomitant changes in the conformation of the PEO chains of the polymer.

3.2.4. Thermal Analysis

In TLC, SCR7 exhibited R_f value of 0.5, SCR7 encapsulated P123 showed two spots with R_f values 0.5 and 0.31. R_f value of 0.31 corresponds to P123. This indicated that there is no chemical interaction between SCR7 and the Pluronic copolymer. Thermal studies indicate a rapid weight-loss occuring for the encapsulated SCR7 around 320 °C. After the end of thermal decomposition, the matrix is burnt completely without leaving behind any residual matter (Figure SV and SVI, Supporting Information). The curves indicate an amorphous or disordered crystalline phase of a molecular dispersion or a solid solution state in the polymer matrix.

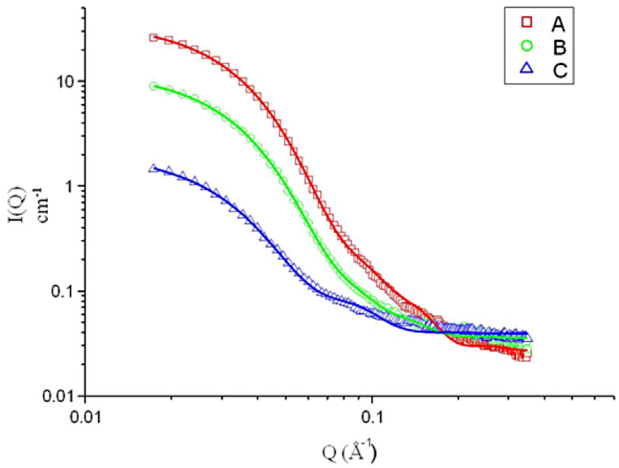

Figure 5. SANS spectra of encapsulated SCR7 at different drug polymer ratios (A) 1:2, (B) 1:4, and (C) 1:40, at a concentration of 1.5% (w/v) in D_2O.

3.3. Cytotoxic Studies

3.3.1. Encapsulated form of SCR7 (ES) induces cytotoxicity in leukemic and breast cancer cells

Cytotoxic potential of ES was evaluated in a leukemic cell line (Nalm6) and breast cancer cell line (MCF7). In both the cases, cells (0.20×10^5) were seeded, and treated after 24 h. The cytotoxicity was determined by Trypan blue and MTT assays after 48 h of treatment. Results showed a dose-dependent increase in the cytotoxicity, when Nalm6 cells were treated with ES (0.05, 0.1. 0.2, 0.5 and 1 mg · ml^{-1}). IC_{50} of encapsulated form of SCR7 in Nalm6 was ca. 0.1 mg · ml^{-1}

Table 1. Variation in micellar parameters with different drug/polymer ratios

Drug/polymer ratio	Core radius [Å]	Shell thickness [Å]
1:40	35	46
1:4	36	47
1:2	30	59

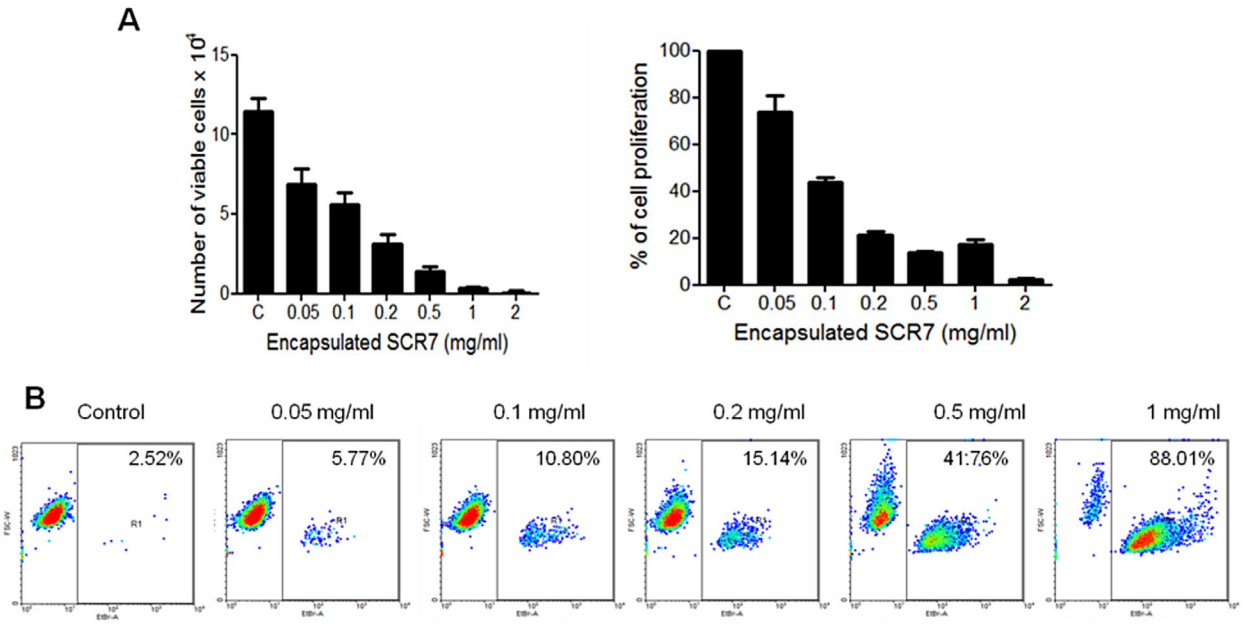

Figure 6. (A) Evaluation of cytotoxic effects of encapsulated form of SCR7 (ES) in leukemic cells. Nalm6 (0.20×10^5) cells were seeded and treated with indicated concentrations of ES for 48 h. Cytotoxicity was evaluated by Trypan blue exclusion and MTT assays. (B). Live-dead cell analysis for estimation of cytotoxic effects exerted by encapsulated form of SCR7 was monitored by ethidium bromide staining.

(Figure 6A). Consistent with this, a dose-dependent increase in cell death was also observed in Nalm6 cells, when live-dead cell assay was performed using flow cytometry (Figure 6B).

To rule out the possibility that the encapsulation matrix used in the preparation of ES causes toxicity by itself, cytotoxicity assays (MTT and trypan blue assays) were carried out by treating Nalm6 cells with increasing concentration of the pluronic polymer (0.05, 0.1. 0.2 and 0.5 $mg \cdot ml^{-1}$) without SCR7 (Figure 7). Results showed no significant decrease in cell viability upon treatment of encapsulation matrix up to 0.1 $mg \cdot ml^{-1}$ concentration, for a period of 48 h (Figure 8). Although higher concentrations induced some degree of cytotoxicity, the amount of matrix present at the IC_{50} concentration (0.1 $mg \cdot ml^{-1}$), did not cause any damage by itself.

Interestingly, MCF7 showed more sensitivity to ES when studied using both MTT and trypan blue assays with an IC_{50} of 0.05 $mg \cdot ml^{-1}$ (Figure 9A). Live-dead cell analysis also showed a significant dose-dependent increase in ethidium

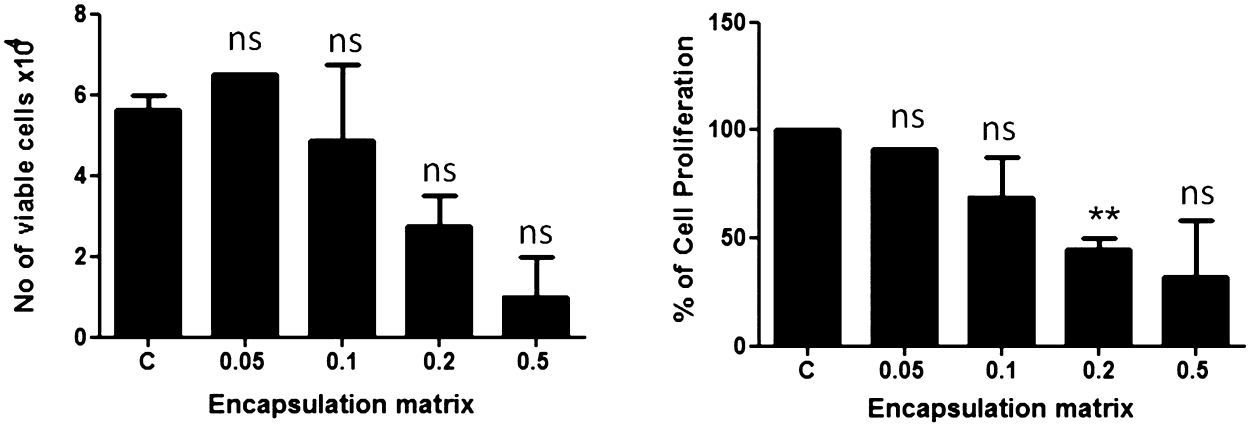

Figure 7. Evaluation of cytotoxic effects of encapsulation matrix (Pluronic P123) in leukemic cells. Nalm6 (0.20×10^5) cells were seeded and treated with indicated concentrations of polymer for 48 h (ns: not significant). Cytotoxicity was evaluated by Trypan blue exclusion and MTT assays.

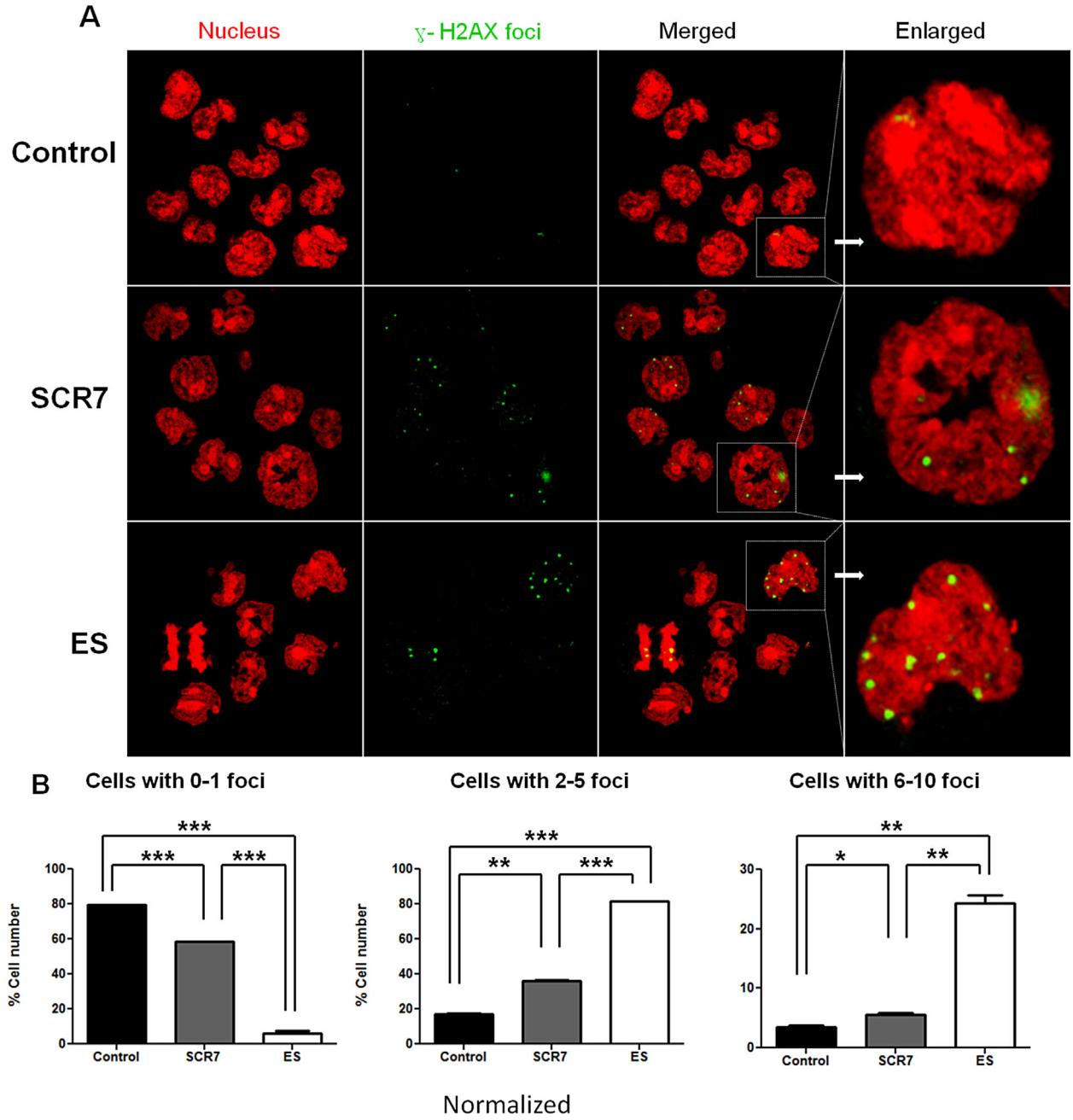

Figure 8. (A) Immunofluorescence showing γ-H2AX foci in Nalm6 cells treated with ES. Nalm6 (0.20×10^5) cells were seeded and treated with 100×10^{-6} M SCR7 and 0.4 mg · ml^{-1} ES. Extent of DNA damage was evaluated by γ-H2AX immunofluorescence after 24 h treatment. (B) Quantification depicting normalized % cell number with indicated number of foci, after SCR7 and ES treatment, based on multiple experiments. (ns: not significant, $^{*}p < 0.05$, $^{**}p < 0.01$, $^{***}p < 0.001$) Normalization was done for ES treated cells, equalizing the amount of SCR7 actually present in the encapsulated form, as compared to SCR7 alone.

bromide stained dead cell population (Figure 9B) further confirming the above results. In a previous study, when parental SCR7 was used, a similar increase in sensitivity towards breast cancer cell lines was also reported.[20] Recently it was established that PEG based copolymers with cisplatin showed dose-dependent cell proliferation inhibition against human breast cancer cell line ZR-75–30.[61]

3.3.2. ES Induces Cell Cycle Arrest at G1 Phase.

DNA damage results in the activation of p53 and checkpoint proteins resulting in cell cycle arrest. As SCR7 is an inhibitor of DNA double-strand break repair, we evaluated the effects of encapsulated form of SCR7 on the cell cycle progression following 48 h of its treatment (Figure 10). Results showed a

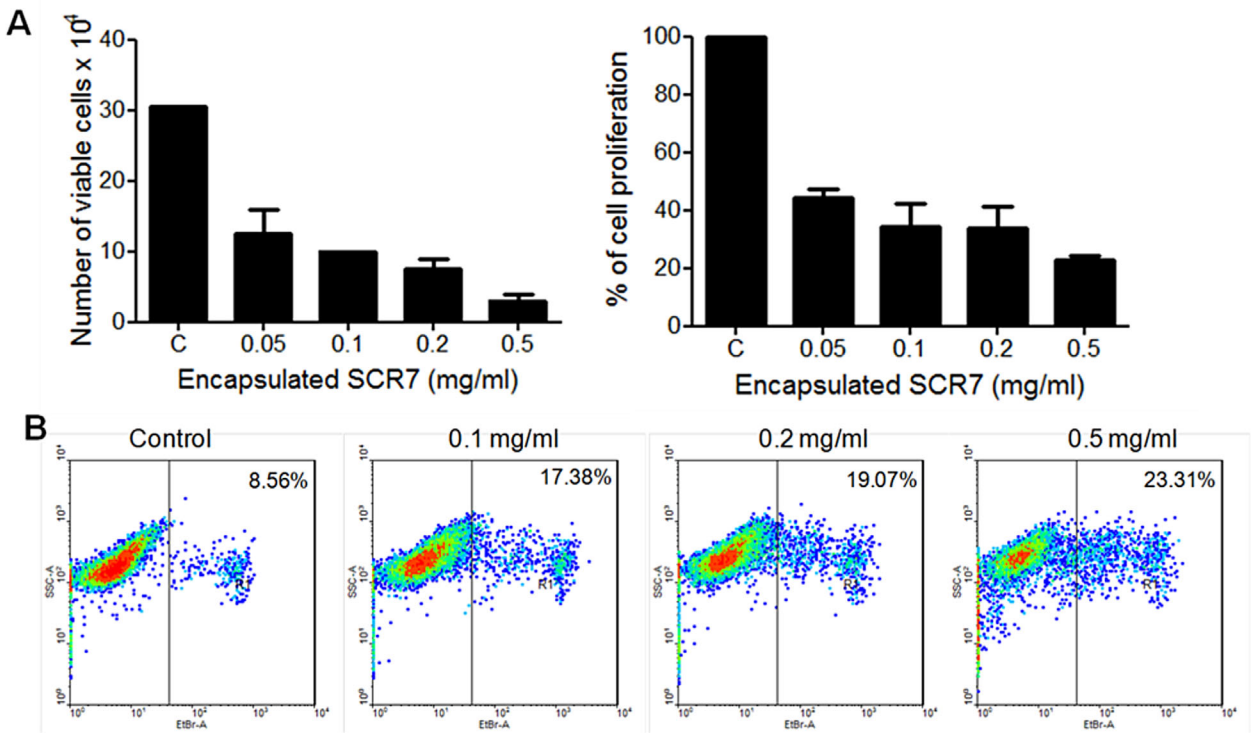

Figure 9. (A) Cytotoxic effects of encapsulated form of SCR7 on breast cancer cell line, MCF7. MCF7 (0.20×10^5) cells were seeded and treated with indicated concentrations of ES for 48 h. Cytotoxicity was evaluated by Trypan blue exclusion and MTT assays. (B). Live-dead cell assay to determine cytotoxic effects caused by copolymer encapsulation on MCF7 cells as monitored by ethidium bromide staining followed by flow cytometry.

prominent arrest at G1 phase of the cell cycle when analysis was done on Nalm6 cells (Figure 10A-C). Cell cycle arrest was predominant at a concentration of 0.1 $mg \cdot ml^{-1}$ of ES (Figure 10A-C). Although a similar G1 arrest was observed even in the case of MCF7 cells, it was less prominent when compared to Nalm6 cells (Figure 10A-D). Although MCF7 was more sensitive to ES in cytotoxicity assays, compared to Nalm6 assays, it was not evident when cell cycle analysis was performed. This difference can be explained by the fact that MTT and Trypan blue assays provide the measure of the live cells, and cannot differentiate between arrested and non-arrested cells. Besides, it should be kept in mind that cell cycle analysis undermines the amount of dead cells for both the cell lines, due to several processing steps involved unlike MTT and Trypan blue assays. Taken together, our results suggested significant G1 arrest in both Nalm6 and MCF7 cells.

3.3.3. ES Induces Apoptosis in Cancer Cells

As encapsulation of SCR7 induces significant cytotoxicity in cancer cell lines, we wanted to decipher its mode of induction of cell death. In order to evaluate weather ES induces apoptotic or necrotic pathways, annexin V/PI double-staining was performed on Nalm6 cells after 48 h of treatment (0, 0.1, 0.2 and 0.5 $mg \cdot ml^{-1}$). The result was a dose-dependent increase in early (annexin positive) and late apoptotic (annexin and PI positive) cell population (Figure 11). Thus our results suggest ES induced apoptosis rather than necrosis, to induce cell death. This result is also consistent with the mode of action of parental SCR7.[20]

Previous studies with SCR7 have shown that it inhibits the NHEJ pathway, activates p53, and brings about cell death by inducing the intrinsic pathway of apoptosis.[20]

3.3.4. ES Leads to the Accumulation of Unrepaired DSBs Within the Cells

Based on cytotoxicity results described above, we were interested in testing whether ES leads to accumulation of DNA damage within the cell, hence inducing apoptosis.

The extent of DNA damage caused by ES was assessed at individual cell level by performing an alkaline Comet assay. Results showed that cells treated with ES (0.4 $mg \cdot ml^{-1}$, for 24 h) harboured extensive DNA damage (Figure 12A). The observed increase in the % DNA in the tail, as well as parameters such as tail moment and Olive moment demonstrated an elevated level of DNA damage (Figure 12B).

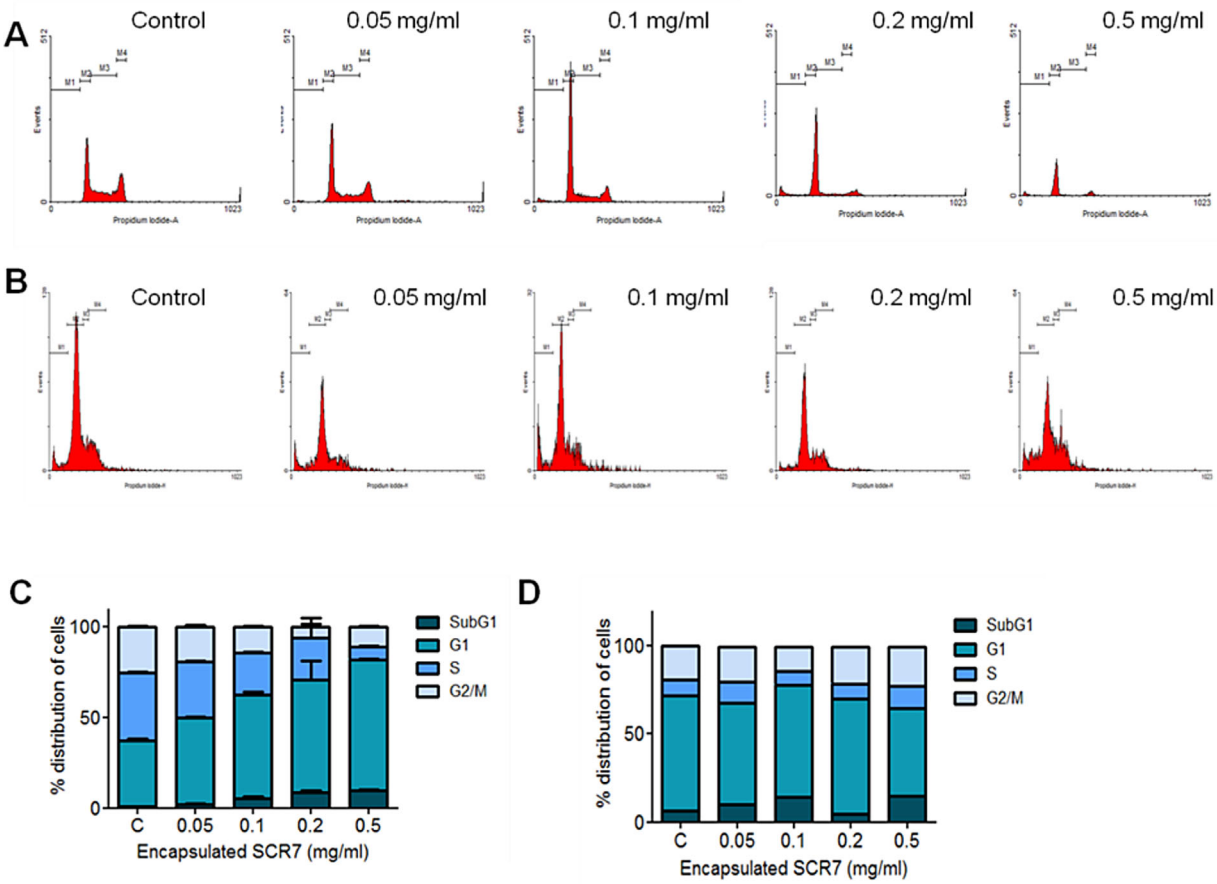

Figure 10. Effect of encapsulated form of SCR7 on cell cycle progression. (A) Cell cycle analysis in Nalm6 and (B) MCF7 cells following treatment with ES (0, 0.05, 0.1, 0.2 and 0.5 mg · ml^{-1}; 48 h). (C) Quantification showing % distribution of Nalm6 and (D) MCF7 cells in different phases of cell cycle following treatment with ES.

DNA damage results in the activation of a cascade pathway termed as the DNA damage response.[62] One of the initial events in this pathway is the phosphorylation of histone H2AX, a variant of the H2A histone family, at serine 139 position, forming distinct foci inside the cell.[63] Upon treatment of Nalm6 cells with ES (0.4 mg · ml^{-1}), increased number of γ-H2AX foci were observed, as compared to untreated cells, indicative of accumulation of unrepaired DSBs within the cell (Figure 8 A). Thus, ES treatment leads to the accumulation of unrepaired DNA breaks within the cell.

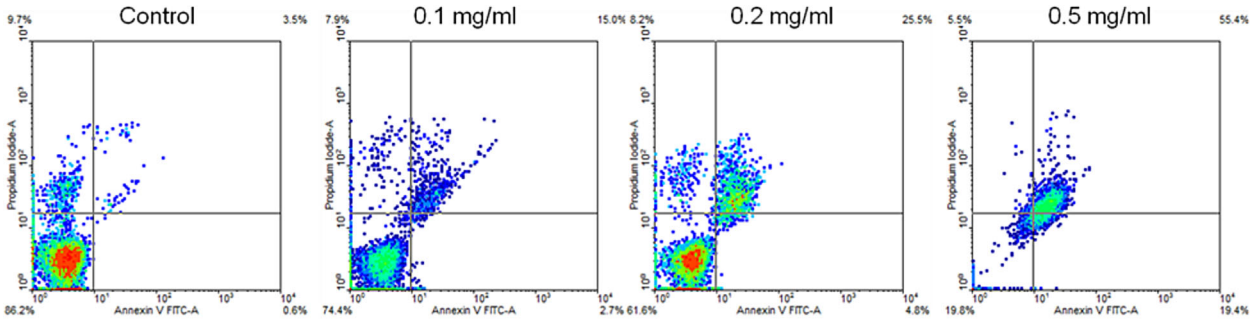

Figure 11. Evaluation of mode of apoptosis following treatment with encapsulated form of SCR7. Nalm6 cells (0.20 × 10^5) were seeded and treated with increasing concentration of ES (0, 0.1, 0.2 and 0.5 mg · ml^{-1}; 48 h). Following staining with Annexin V-FITC/Propidium Iodide, mode of apoptosis was assayed using flow cytometry.

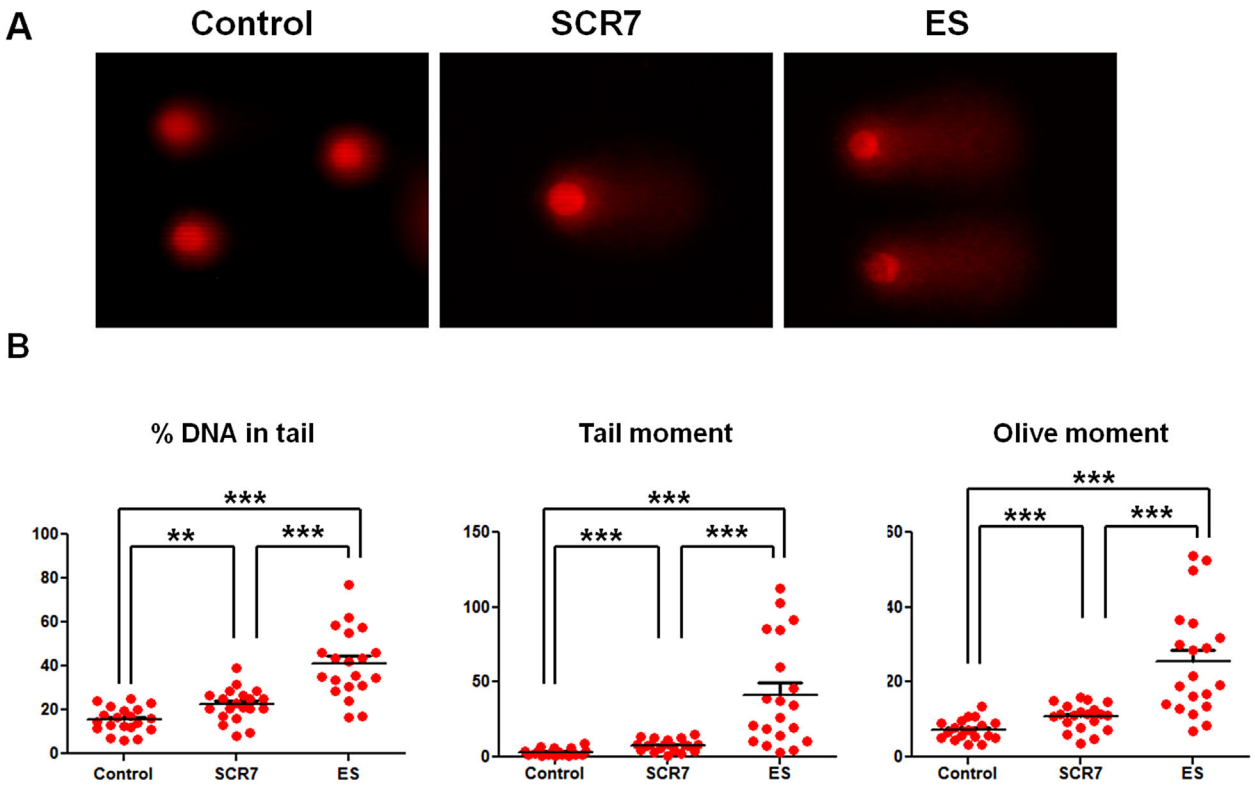

Figure 12. (A) Evaluation of direct DNA damage induced by ES using Comet assay. Nalm6 (0.20×10^5) cells were seeded and treated with 100×10^{-6} M SCR7 and 0.4 mg · ml^{-1} ES for 24 h and the extent of DNA damage was evaluated by alkaline comet assay. (B) Quantification depicting amount of DNA breaks in the cells after treatment, for different parameters such as % DNA damage, tail moment and Olive moment (ns: not significant, $^*p < 0.05$, $^{**}p < 0.01$, $^{***}p < 0.001$).

A comparative analysis of the efficacy of SCR7 and its encapsulated form (ES), showed that a 5-fold lower concentration of SCR7 was sufficient to exhibit similar cytotoxic effects in cells, when used as encapsulated form in Nalm6 cells. The comparison was also extended for the extent of DNA damage induced within the cell. γ-H2AX immunofluorescence results showed a 4-fold increase in cells bearing 6–10 foci in ES treated samples, as compared to SCR7 treatment (Figure 8 B). Comet assay analysis showed increased percentage of DNA in the tail in ES treated cells, as compared to SCR7 treated ones.

Among different strategies used for targeting cancer cells, inhibition of a particular DNA repair pathway in cells, is gaining importance in recent times.[64,10] Although normal cells possess such DNA repair pathways as well, this strategy takes advantage of the fact that cancer cells possess higher innate DNA breaks, and a faster proliferation rate, thus rendering selectivity.[65] SCR7, an inhibitor of DNA Ligase IV, has been shown to cause accumulation of unrepaired DNA breaks inside the cell, resulting in activation of apoptosis in cancer cells. One of the drawbacks of SCR7 has been its hydrophobic nature, which makes it poorly soluble in water, thus limiting bio-availability. Here, we adopted the encapsulation of SCR7 with Pluronic P123 co-polymer, resulting in nano-dimensional micelle and showed its increased availability, within the cells.

Like SCR7, upon ES treatment, we observed significant increase in the accumulation of unrepaired DSBs within the cell, indicating abrogation of NHEJ, activation of p53-mediated intrinsic apoptotic pathway, and eventually cell death, with increased efficacy as compared to SCR7. Previous studies have shown that treatment of cells with SCR7 leads to the phosphorylation of Ataxia telangiectasia mutated (ATM) kinase, which in turn phosphorylates p53, resulting in activation of the p53 mediated intrinsic pathway of apoptosis.[20] Since p53 is either lost or mutated in 50% of all cancer types, it would be interesting to study the effect of ES in such cancers in order to exploit its antioxidative weakness.[66]

One of the disadvantages of using nano materials is that it can trigger latent toxicity, leading to impaired cellular function.[67] Metal nanoparticles can engage regulation of p53 through intracellular reactive oxygen species (ROS). Excessive accumulation of ROS may promote tumor incidence which is a setback in cancer therapy.[66] However, micellar encapsulation of SCR7 produces particles in the nanometer range and induced only minimal cytotoxicity, as indicated by cellular assays.

Although usage of nanomaterials as carriers has been the traditional route to nanomedicine, recent studies have also explored the possibility of the nano carrier itself acting as a drug. One such example is the use of ZnO nanoparticles, which have been shown to exploit the p53 status of a cell, thus rendering specificity to cancer cells, while sparing normal cells.[68] It would be interesting to employ a combination strategy, wherein potent anti-cancer molecules like SCR7 could be encapsulated with such nanomaterials, giving it a more efficient, dual mode of action.

In the field of anti-cancer therapeutics in recent times, major focus has been towards efficient killing of cancer cells without any side-effects. This involves adopting a technology that produces maximum effect with a minimal concentration or dose (in case of radio-therapy). Interestingly, our studies indicate that encapsulation of SCR7 rendered it around 5 times more potent as compared to the parental compound. This finding opens up a new avenue for the use of the modified form of SCR7 against different cancers. Previous studies have shown that SCR7 can potentiate the effect of radiation in anti-cancer therapy.[20] Our new finding suggests that the dose of SCR7 can be further brought down, due to efficient bio-availability of the molecule when it is in encapsulated form. Thus, use of ES SCR7 serves as a promising technology for development of potent anti-cancer treatment modalities.

One of the leading cancer therapeutics strategies includes combination therapy, where multiple drugs targeting the same or different pathways are used in order to increase the efficacy of treatment.[69] Previously it has been shown that in a combination therapy, SCR7, along with either ionizing radiation or etoposide, successfully enhanced tumor regression in mice as compared to individual treatments.[20] Although drug combinations are synergistic, there are possibilities that some drugs may act in an antagonistic manner when used in combination. However, recent studies highlight the advantage of encapsulation of drugs to avoid antagonism.[70] Thus, the potential anti-cancer effect of ES can further be explored for combination therapy along with a number of frontline drugs such as cisplatin, doxorubicin, paclitaxel, etc.[22,61]

Thus the clinical development of this polymer-drug conjugate as a new class of anticancer agent would be a continuous concerted effort at the interface of chemistry and biology for in vivo application. The biocompatibility of the polymeric matrix can serve as an ideal formulation for tissue engineering and controlled drug delivery applications.

4. Conclusion

Newly synthesized anti cancer agent SCR7 has the capability to inhibit NHEJ in a Ligase IV dependent manner within cells. Hydrophobicity of SCR7 decreases its bioavailability, which is a major setback in utilization of this compound as a therapeutic agent. Polymer encapsulation of small molecules to enhance the physicochemical properties represents an intriguing approach in recent drug discovery. The focus of the reported study is to formulate an aqueous soluble matrix for efficient delivery of SCR7. Thin film hydration method is confirmed to be one of the most suitable methods for the encapsulation of SCR7 in a Pluronic matrix. ^{1}H NMR spectrum confirmed the entrapment of the drug within the polymeric core, along with fluorescence, UV-Vis and FT-IR spectroscopic techniques. SCR7 is efficiently diffused from the polymeric core as evidenced from the chloroform extract. TEM, DLS and SANS results demonstrated that Pluronic polymer could very well be used as an efficient carrier for hydrophobic molecule such as SCR7. The in vitro cytotoxic assays showed that the encapsulated form of SCR7 induced cytotoxicity in a concentration dependent manner. Importantly, encapsulated SCR7 treatment led to arrest at G1 phase of the cell cycle, thus culminating into apoptosis. γ-H2AX immunofluorescence and comet assay analysis showed that ES treatment led to accumulation of unrepaired DSBs within the cell, thus inducing apoptosis. Taken together, our data suggests that encapsulation of SCR7 can effectively induce cytotoxicity in cancer cell lines by inducing cell cycle arrest, leading to apoptosis. Moreover, a comparative analysis of the efficacy of SCR7 and ES, showed that encapsulation rendered the molecule ≈5 times more effective than its hydrophobic counterpart.

Acknowledgements: The authors are grateful to Sophisticated Instrumentation Facility, CUSAT, Kochi for the analytical instrumentation service. Fluorescence and TOF MS/MS spectra were recorded at School of Environmental Sciences, M. G. University, Kottayam. We thank Indian Institute of Science, FACS facility for their help in flow cytometric studies. FJ and JG thank Department of Biotechnology, Govt. of India (DBT, No. BT/PR7703/27/493/2013) for financial support. SCR acknowledges financial assistance from IISc-DBT partnership programme [DBT/BF/PR/INS/2011-12/IISc] and IISc, Bangalore. SV and MS are supported by JRF and postdoctoral fellowship from IISc.
Note: The name of author S. V. Vartak was mistakenly omitted from the affiliations in the original version of this article. The affiliation information for author S. V. Vartak was added on April 13, 2015.

Received: October 31, 2014; Revised: November 14, 2014; Published online: December 16, 2014; DOI: 10.1002/mabi.201400480

Keywords: pluronic block copolymer; polymeric micelles; SCR7

[1] J. Ferlay, H. R. Shin, F. Bray, D. Forman, C. Mathers, D. M. Parkin, *Int. J. Cancer* **2010**, *127*, 2893.

[2] J. Luo, N. L. Solimini, S. J. Elledge, *Cell* **2009**, *136*, 823.
[3] C. L. Chaffer, R. A. Weinberg, *Science* **2011**, *331*, 1559.
[4] P. Aris, *Nat. Biotechnol.* **1999**, *17*, 94.
[5] M. M. Gottesman, T. Fojo, S. E. Bates, *Nat. Rev. Cancer* **2002**, *2*, 48.
[6] D. M. Molina, R. Jafari, M. Ignatushchenko, T. Seki, E. A. Larsson, C. Dan, L. Sreekumar, Y. Cao, P. Nordlund, *Science* **2013**, *341*, 84.
[7] S. Aggarwal, *Nat. Rev. Drug Discov.* **2010**, *9*, 427.
[8] H. A. Shih, J. S. Loeffler, N. J. Tarbell, Late Effects of CNS Radiation Therapy. *Late Effects of Treatment for Brain Tumors*, Springer, Berlin **2009**. p. 23.
[9] S. P. Jackson, J. Bartek, *Nature* **2009**, *461*, 1071.
[10] T. Helleday, E. Petermann, C. Lundin, B. Hodgson, R. A. Sharma, *Nat. Rev. Cancer* **2008**, *8*, 193.
[11] S. Sharma, B. Choudhary, S. C. Raghavan, *Cell. Mol. Life Sci.* **2011**, *68*, 661.
[12] M. R. Lieber, K. Yu, S. C. Raghavan, *DNA Repair* **2006**, *5*, 1234.
[13] C. Wyman, R. Kanaar, *Annu. Rev. Genet.* **2006**, *40*, 363.
[14] V. Gopalakrishnan, S. C. Raghavan, *Future Oncol.* **2012**, *8*, 1121.
[15] M. Nambiar, S. C. Raghavan, *Cell. Mol. Life Sci.* **2013**, *70*, 1381.
[16] M. Nambiar, S. C. Raghavan, *Nucleic Acids Res.* **2011**, *39*, 5813.
[17] S. C. Raghavan, P. C. Swanson, X. Wu, C. L. Hsieh, M. R. Lieber, *Nature* **2004**, *428*, 88.
[18] F. W. Alt, Y. Zhang, F. L. Meng, C. Guo, B. Schwer, *Cell* **2013**, *152*, 417.
[19] M. L. Hefferin, A. E. Tomkinson, *DNA Repair* **2005**, *4*, 639.
[20] M. Srivastava, M. Nambiar, S. Sharma, S. S. Karki, G. Goldsmith, M. Hegde, S. Kumar, M. Pandey, R. K. Singh, P. Ray, R. Natarajan, M. Kelkar, A. De, B. Choudhary, S. C. Raghavan, *Cell* **2012**, *151*, 1474.
[21] R. B. Campbell, S. V. Balasubramanian, R. M. Straubinger, *J. Pharm. Sci.* **2001**, *90*, 1091.
[22] H. F. Wang, H. Z. Jia, Y. F. Chu, J. Feng, X. Z. Zhang, R. X. Zhuo, *Macromol. Biosci.* **2014**, *14*, 526.
[23] I. F. Uchegbu, S. P. Vyas, *Int. J. Pharm.* **1998**, *172*, 33.
[24] T. Nakanishi, S. Fukushima, K. Okamoto, M. Suzuki, Y. Matsumura, M. Yokoyama, T. Okano, Y. Sakurai, K. Kataoka, *J. Controlled Release* **2001**, *74*, 295.
[25] M. Ferrari, *Nat. Rev. Cancer* **2005**, *5*, 161.
[26] R. B. Greenwald, C. D. Conover, Y. H. Choe, *Crit. Rev. Ther. Drug Carrier Syst.* **2000**, *17*, 101.
[27] M. A. Moses, H. Brem, R. Langer, *Cancer Cell* **2003**, *4*, 337.
[28] R. Langer, N. A. Peppas, *AIChE J.* **2003**, *49*, 2990.
[29] E. M. Martin, M. A. del Valle, R. G. Galan, Carbonell, *Ind. Eng. Chem. Res.* **2009**, *48*, 2475.
[30] T. Feczko, *Recent Pat. Mater. Sci.* **2009**, *2*, 32.
[31] X. Jiang, E. B. Vogel, M. R. Smith, G. L. Baker, *Macromolecules* **2008**, *41*.
[32] J. Green, Z. Tyrrell, M. Radosz, *J. Phys. Chem. C* **2010**, *114*, 16082.
[33] K. Cui, D. D. Zhu, W. Cui, X. M. Lu, Q. H. Lu, *J. Phys. Chem. C* **2012**, *116*, 6077.
[34] Y. Qiu, K. Park, *Adv. Drug Delivery Rev.* **2001**, *53*, 321.
[35] H. Sai, K. W. Tan, K. Hur, E. A. Smith, R. Hovden, Y. Jiang, M. Riccio, D. A. Muller, V. Elser, L. A. Estroff, S. M. Gruner, U. Wiesner, *Science* **2013**, *341*, 530.
[36] A. K. Bajpai, S. K. Shukla, S. Bhanu, S. Kankane, *Prog. Polym. Sci.* **2008**, *33*, 1088.
[37] Y. Kadam, R. Ganguly, M. Kumbhakar, K. Aswal, P. A. Hassan, P. Bahadur, *J. Phys. Chem. B* **2009**, *113*, 16296.
[38] S. Alexander, M. W. de Vos, T. C. Castle, T. Cosgrove, S. W. Prescott, *Langmuir* **2012**, *28*, 6539.
[39] V. Y. Alakhov, E. Moskaleva, E. V. Batrakova, A. V. Kabanov, *Bioconjug. Chem.* **1996**, *7*, 209.
[40] C. Dumontet, M. A. Jordan, *Nat. Rev. Drug Discov.* **2010**, *9*, 790.
[41] A. Musyanovych, K. Landfester, *Macromol. Biosci.* **2014**, *14*, 458.
[42] W. Zhang, Y. Shi, C. Yanzuo, Y. Shuangyin, H. Junguo, L. Jieqi, S. Xianyi, F. Xiaoling, *Eur. J. Pharm. Biopharm.* **2010**, *75*, 341.
[43] Y. Wang, L. Yu, L. Han, X. Sha, X. Fang, *Int. J. Pharm.* **2007**, *337*, 63.
[44] I. V. Chernushevich, A. V. Loboda, B. A. Thomson, *J. Mass. Spectrom.* **2001**, *36*, 849.
[45] M. J. Ansari, S. Ahmad, K. Kholi, J. Ali, R. K. Khar, *J. Pharm. Biomed. Anal.* **2005**, *39*, 132.
[46] C. V. Kavitha, M. Nambiar, P. B. Narayanaswamy, E. Thomas, U. Rathore, C. S. A. Kumar, B. Choudhary, K. S. Rangappa, S. C. Raghavan, *PLoS One* **2013**, *8*, e.
[47] M. S. Shahabuddin, M. Nambiar, B. T. Moorthy, P. L. Naik, B. Choudhary, G. M. Advirao, S. C. Raghavan, *Invest. New Drugs* **2011**, *29*, 523.
[48] V. L. Hegde, P. S. Nagarkatti, M. Nagarkatti, *PLoS One* **2011**, *6*, e18281.
[49] K. K. Chiruvella, V. Kari, B. Choudhary, M. Nambiar, R. G. Rama, G. Ghanta, S. C. Raghavan, *FEBS Lett.* **2008**, *582*, 4066.
[50] S. Sharma, K. Panjamurthy, B. Choudhary, M. Srivastava, M. S. Shahabuddin, R. Giri, G. M. Advirao, S. C. Raghavan, *Mol. Carcinog.* **2013**, *52*, 413.
[51] M. S. Shahabuddin, M. Nambiar, G. M. Advirao, S. C. Raghavan, *Invest. New Drugs* **2011**, *29*, 873.
[52] P. L. Olive, J. P. Banáth, *Nat. Protoc.* **2006**, *1*, 23.
[53] G. Y. Liu, M. Li, C. S. Zhu, Q. Jin, Z. C. Zhang, J. Ji, *Macromol. Biosci.* **2014**, *14*, 1280.
[54] S. Sanyakamdhorn, D. Agudelo, H. A. Tajmir-Riahi, *Biomacromolecules* **2013**, *14*, 557.
[55] A. Sahu, N. Kasoju, U. Bora, *Biomacromolecules* **2008**, *9*, 2905.
[56] L. M. Huong, H. P. Thu, T. B. T. Nguyen, T. H. H. Tran, T. M. T. Ha, M. T. Trang, T. Q. Duong, *Chem. Lett.* **2011**, *40*, 846.
[57] J. W. Lee, E. D. Jeong, E. J. Cho, J. A. Gardella Jr., W. Hicks Jr., R. Hard, F. V. Bright, *Appl. Surf. Sci.* **2008**, *255*, 2360.
[58] D. Qiu, C. Flood, T. Cosgrove, *Langmuir* **2008**, *24*, 2983.
[59] S. Alexander, T. Cosgrove, T. C. Castle, I. Grillo, S. W. Prescott, *J. Phys. Chem. B* **2012**, *116*, 11545.
[60] P. Alexandridis, L. Yang, *Macromolecules* **2000**, *33*, 5574.
[61] Z. Ahmad, Z. Tang, A. Shah, S. Lv, D. Zhang, Y. Zhang, X. Chen, *Macromol. Biosci.* **2014**, *14*, 1337.
[62] S. P. Jackson, J. Bartek, *Nature* **2009**, *461*, 1071.
[63] A. Sharma, K. Singh, A. Almasan, *Methods Mol. Biol.* **2012**, *920*, 613.
[64] M. Srivastava, S. C. Raghavan, *Chem. Biol.* **2014**, (in press).
[65] A. C. Begg, F. A. Stewart, C. Vens, *Nat. Rev. Cancer* **2011**, *11*, 239.
[66] M. I. Setyawati, C. Y. Tay, D. T. Leong, *Nanomedicine* **2014**, *9*, 369.
[67] C. Y. Tay, M. I. Setyawati, J. Xie, W. J. Parak, D. T. Leong, *Adv. Funct. Mater.* **2014**, *24*, 5936.
[68] K. W. Ng, S. P. K. Khoo, B. C. Heng, M. I. Setyawati, E. C. Tan, X. Zhao, S. Xiong, W. Fang, D. T. Leong, J. S. C. Loo, *Biomaterials* **2011**, *32*, 8218.
[69] X. Su, C. Dong, J. Zhang, L. Su, X. Wang, H. Cui, Z. Chen, *Cell & Biosci.* **2014**, *4*, 7.
[70] G. R. Tan, S. S. Feng, D. T. Leong, *Biomaterials* **2014**, *35*, 3044.

Faraday Discussions

Cite this: *Faraday Discuss.*, 2015, **177**, 155

PAPER

Pluronic copolymer encapsulated SCR7 as a potential anticancer agent

Franklin John,*[a] Jinu George,[a] Mrinal Srivastava,[b] P. A. Hassan,[c] V. K. Aswal,[d] Subhas. S. Karki[e] and Sathees. C. Raghavan[b]

Received 15th September 2014, Accepted 4th November 2014

DOI: 10.1039/c4fd00176a

Nonhomologous end joining (NHEJ) of DNA double strand breaks (DSBs) inside cells can be selectively inhibited by 5,6-bis-(benzylideneamino)-2-mercaptopyrimidin-4-ol (SCR7) which possesses anticancer properties. The hydrophobicity of SCR7 decreases its bioavailability which is a major setback in the utilization of this compound as a therapeutic agent. In order to circumvent the drawback of SCR7, we prepared a polymer encapsulated form of SCR7. The physical interaction of SCR7 and Pluronic® copolymer is evident from different analytical techniques. The *in vitro* cytotoxicity of the drug formulations is established using the MTT assay.

Introduction

Cancer drug targeting is challenged by problems like multi-drug resistance and low solubility of potential drug candidates. There are two general classes of resistance to anti-cancer drugs: those that impair delivery of anti-cancer drugs to tumor cells, and those that arise in the cancer cell itself due to genetic and epigenetic alterations that affect drug sensitivity. Impaired drug delivery can result from poor absorption of orally administered drugs, increased drug metabolism or increased excretion, resulting in lower levels of drug in the blood and reduced diffusion of drugs from the blood into the tumor.[1,2]

Cytotoxic therapy offers one prominent approach towards cancer treatment. Traditional cytotoxic therapy includes radiation and chemotherapeutic compounds such as platinum-based drugs.[3–6] Among the genetic damages, DNA double strand breaks (DSBs) are considered as the most lethal as they affect the integrity and continuity of the genome.[7–10] Inappropriate repair of DSBs may result in deletions, inversions, duplications and chromosomal translocations.[11–14]

[a]*Biotechnology Laboratory, PG and Research Department of Chemistry, Sacred Heart College, Kochi 682 013, India. E-mail: franklinshc@gmail.com*

[b]*Department of Biochemistry, Indian Institute of Science, Bangalore 560 012, India*

[c]*Chemistry Division, Bhabha Atomic Research Centre, Mumbai 400 085, India*

[d]*Solid State Physics Division, Bhabha Atomic Research Centre, Mumbai 400 085, India*

[e]*Department of Pharmaceutical Chemistry, KLE University, Bangalore 560 010, India*

Nonhomologous DNA end joining (NHEJ) is one of the major DNA DSB repair pathways.[15] Recently, a novel inhibitor of NHEJ, 5,6-bis-(benzylideneamino)-2-mercaptopyrimidin-4-ol (SCR7) has been reported.[16] Inhibition of NHEJ by SCR7 in cancer cells results in the accumulation of unrepaired DNA double-strand breaks. Despite promising results of SCR7 as a good anticancer agent, it showed high IC_{50} which could be attributed to its high hydrophobicity.

Results and discussion

Although SCR 7 has shown promising results as a potential anticancer drug, its limited solubility in water may lead to poor bioavailability and requires the search for novel drug delivery systems. Traditional methods to improve the bioavailability of poorly soluble drugs include encapsulating them in nanosized carriers such as liposomes,[17] emulsions, polymer micelles, niosomes,[18] lipid particles *etc.* Poly Ethylene Glycol (PEG)[19] based block copolymers have the distinct advantage as compared to other delivery systems due to its ability to encapsulate large amounts of drug. One of the most widely studied classes of amphiphilic copolymers in this field is the Pluronic triblock copolymers. Thus, we investigated the role of Pluronic P123 in encapsulating and delivering SCR7 *via* hydrophobic interactions.

Fluorescence emission spectra of SCR7 showed a blue shift upon encapsulation with P123 copolymer in DMSO as solvent as shown in Fig. 1(a). The fluorescence spectra of SCR7 in DMSO exhibits an emission peak at ~474 nm while SCR7 in the presence of P123 show a maximum at ~442 nm with the same solvent (DMSO due to the high solubility of SCR7).[20] The shift in the λ_{max} of fluorescence spectrum is an indication of interaction between SCR7 and the copolymer P123. Such shift in the fluorescence emission is reported for doxorubicin encapsulated with chitosan nano particles and curcumin casein micelles.[21,22]

Fig. 1(b) shows the UV-Vis absorption spectra of SCR7-P123 dissolved in a minimum amount of water. The hydrophobic PPO core of the copolymer effectively encapsulates the drug molecule and makes it dispersible in the aqueous layer. To reiterate the encapsulation and release of SCR7 from P123, the aqueous

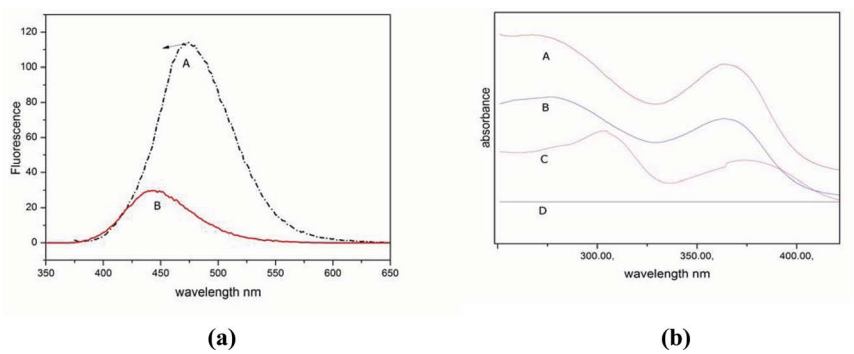

Fig. 1 (a) (A) Fluorescence emission spectra of SCR7 in DMSO (B) SCR7 loaded P123 in DMSO. (b) (A) UV absorption spectra of SCR7 loaded P123 in water (B) chloroform extract (C) SCR7 alone in water (D) P123 in water.

layer was extracted with chloroform (3×). The chloroform layer is dried with Na_2SO_4. UV absorption spectra of the chloroform layer show absorption maxima at 267 nm and 365 nm. The optical absorption spectrum of the chloroform layer is compared with SCR7 in pure water and SCR7 encapsulated P123 in water (A and C of Fig. 1(b)). This indicates the ability of P123 in encapsulating the drug and its release upon treatment with hydrophobic solvents like chloroform.

The FTIR spectra of SCR7 and SCR7 encapsulated with P123 are depicted in Fig. 2. The C–S stretching vibrations occur at 3271 cm^{-1}, while the C–S bending occurs at 1047 cm^{-1} and 1082 cm^{-1}. The C–N stretching vibrations occur at 1026 cm^{-1}, whereas the N–H bending vibrations occur at 924 cm^{-1}. The absorptions at 1250 cm^{-1}, 1117.6 cm^{-1} and 1031.1 cm^{-1} are due to C–O stretching vibrations from the P123 matrix. The absorptions at 957 cm^{-1} and 817 cm^{-1} are arising from the aromatic ring of SCR7. As seen, the spectrum of SCR7-P123 did show the characteristic absorption band of SCR7 at 2965 cm^{-1} and 1107 cm^{-1}. FT-IR spectral analysis reveals that there is no appreciable shift in the IR signal of SCR7 when it changes from the free state to the polymer bound state. It can also be concluded that there is no chemical interaction taking place between P123 and SCR7. The result confirmed the presence of SCR7 in the encapsulated formulation.

Successful incorporation of SCR7 in P123 and its release in different solvents was elucidated by ^{1}H NMR spectroscopy. As is evident from Fig. 3, the ^{1}H NMR spectra of SCR7-P123 employing DMSO-d6 as the solvent showed characteristic aromatic signals from SCR7 at 7.1–7.5 ppm. In all the spectra, the aromatic proton signals corresponding to SCR7 are seen with lower intensity than compared with the Pluronic counterpart. The small signals from SCR7 are indicated by * in Fig. 3.

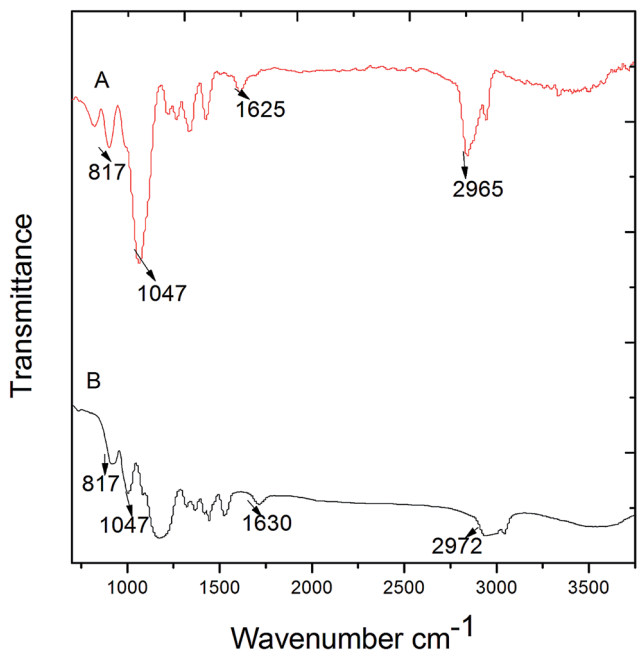

Fig. 2 FT-IR spectra of (A) SCR7 and (B) SCR7-P123.

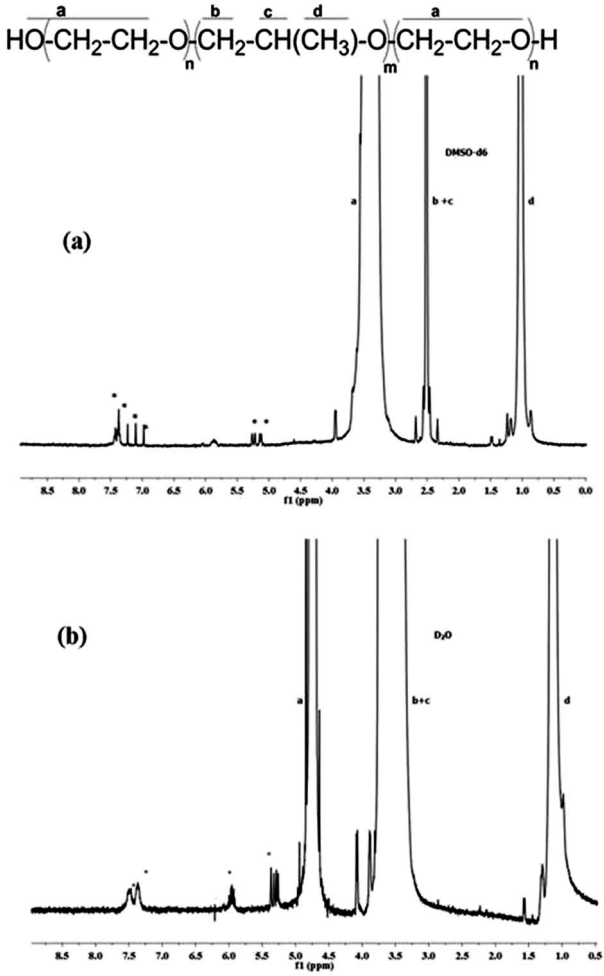

Fig. 3 ^{1}H NMR spectra of SCR7P123 in (a) DMSO-d6 (b) D_2O.

In vitro cytotoxic assay

A cytotoxic assay was performed to measure the metabolic activity of cells. This was carried out by reducing yellow coloured tetrazolium salt 3-(4,5-dimethyl thiazol-2-yl)-2,5-diphenyltetrazolium bromide to purple coloured formazan. The test sample was prepared by dissolving 200 mg of SCR7-P123 in 0.5 mL of DMSO and made up to 5.8 mL with culture medium containing serum and sterilized filters. This was diluted with culture medium to 50%, 25% and 12.5%. Cells cultured in normal medium were considered as the cell control. An equal volume (100 μL) of various dilutions of test samples, extract of negative control, cell control and positive control were placed on subconfluent monolayer of L929 cells. After incubation of the cells with various concentrations of test sample and controls at 37 °C for 24 ± 2 h, the extract and control medium was replaced with 50 μL MTT solution (1 mg mL^{-1} in medium without supplements), wrapped with

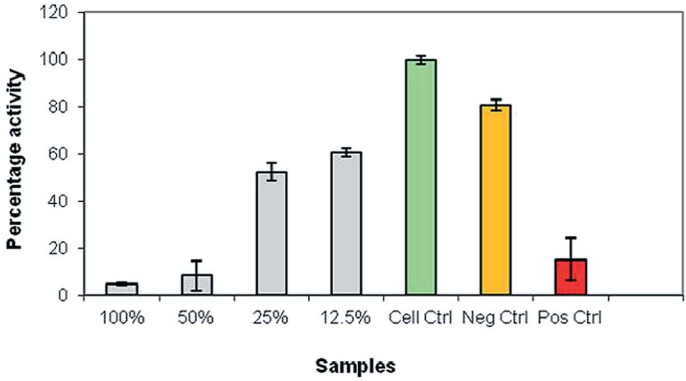

Fig. 4 MTT assay profile of SCR7P123.

aluminium foil and incubated at 37 °C for 2 hours. After discarding the MTT solution 100 μL of isopropanol was added to all wells and the plates were shaken. The developed colour was quantified by measuring absorbance at 570 nm using a spectrophotometer. The data obtained for the test sample were compared with the cell control. As shown in Fig. 4, the MTT assay of L929 cells after 24 hour contact with samples 100%, 50%, 25% and 12.5% of test material SCR7P123 showed 4.72%, 8.23%, 52.29%, and 60.69% metabolic activity respectively. The positive control (diluted phenol with culture medium containing serum) showed 15.14% and the negative control (ultra high molecular weight poly ethylene with culture medium containing serum) showed 80.56% metabolic activity.

Experimental section

Pluronic P123 and D_2O were purchased from Aldrich (Bangalore, India). All the salts and solvents used in the study were purchased from Merck (Mumbai, India). All other reagents and buffer solution components were analytical grade. Distilled and deionized water was used in all experiments.

Preparation of SCR7-loaded polymeric micelles

SCR7 loaded micelles were prepared by the thin-film hydration method. 8 mg of SCR7 and 440 mg of Pluronic block copolymer were dissolved in 10 mL acetonitrile in a round-bottom flask. The solvent was evaporated by rotary evaporation at 50 °C for about 1 h to obtain a solid SCR7-P123 matrix. Residual acetonitrile remaining in the film was removed under vacuum overnight at room temperature. Then, the resultant thin film was hydrated with different amounts of water, while the hydration temperature was varied according to the experimental design. The mixture was stirred at 700 rpm for 30 min to obtain a micelle solution, which was then filtrated through 0.2 μm filter membrane to remove the unincorporated drug aggregates, followed by lyophilization.

Characterization

Fluorescence emissions were recorded on a F-2500 fluorescence spectrometer (Hitachi, Japan). UV measurements were performed on a Shimadzu (UV-2450) UV-

visible double beam spectrophotometer with a matched pair of stoppered fused silica cells of 1 cm optical path length. Fourier transformed infrared (FT-IR) measurements were obtained using a SHIMADZU 8400 FT IR spectrometer. The drug loading and release characteristics of P123 encapsulated SCR7 was analyzed by ^{1}H NMR spectra which was recorded on a Varian 400 MHz spectrometer (Varian, Palo Alto, CA, USA) in deuterated dimethyl sulfoxide (DMSO-d6), chloroform ($CDCl_3$) and water (D_2O) at room temperature.

Thin layer chromatography (TLC) was adopted to study the physical interaction of SCR7 and P123. 10% methanol in chloroform was used as the mobile phase and silica gel G was used as the stationary phase. The spots were detected under UV light and stained using alkaline $KMnO_4$ solution and the R_f values were determined.[23] To evaluate the cell cytotoxic potential of SCR7-P123, a MTT assay was performed. The cell line was obtained from the biotechnology wing of SCTIMST Thiruvananthapuram. The source of the cell line is the ATCC strain and L-929. L-929 is an established and well characterized mammalian cell line that has demonstrated reproducible results. The cells were cultured in 10% FBS. Ultra high molecular weight poly ethylene was used as the negative control and it was prepared by incubating 3 cm^2 ultra high molecular weight poly ethylene with culture medium containing serum at 37 $\pm$ 1 °C for 24 $\pm$ 2 h. Diluted phenol was used as the positive control and was prepared by diluting phenol stock solution (13 mg mL^{-1}) to 1.3 mg mL^{-1} with culture medium containing serum.

Conclusions

Anti cancer agent SCR7 has the capability to inhibit NHEJ in a Ligase IV dependent manner within cells. Hydrophobicity of SCR7 is a major setback in the utilization of this compound. Polymer encapsulation of small molecules to enhance their physicochemical properties represents an alternative approach in recent drug discovery research. The major focus of the reported study is to formulate an aqueous soluble matrix for drug delivery. The thin film hydration method is confirmed to be one of the most suitable methods for the encapsulation of SCR7 within the copolymer. ^{1}H NMR spectra confirmed the entrapment of the drug within the Pluronic polymeric core, along with fluorescence, UV-Vis and FT-IR spectroscopic techniques. SCR7 is efficiently diffused from the polymeric core as evidenced from the chloroform extract. *In vitro* cytotoxic assays showed that the encapsulated form of SCR7 induced cytotoxicity in a concentration dependent manner. Biocompatibility of the polymeric matrix can serve as an ideal formulation for controlled drug delivery applications.

Acknowledgements

The authors thank Department of Biotechnology, Govt. of India (DBT, no. BT/PR7703/27/493/2013) for financial support. We are grateful to Sophisticated Instrumentation Facility, CUSAT, Kochi for the analytical instrumentation service. Fluorescence and TOF MS/MS spectra were recorded at School of Environmental Sciences, M.G University, Kottayam.

Notes and references

1 M. M. Gottesman, T. Fojo and S. E. Bates, *Nat. Rev. Cancer*, 2002, **2**, 48.
2 D. M. Molina, R. Jafari, M. Ignatushchenko, T. Seki, E. A. Larsson, C. Dan, L. Sreekumar, Y. Cao and P. Nordlund, *Science*, 2013, **341**, 84.
3 S. Aggarwal, *Nat. Rev. Drug Discovery*, 2010, **9**, 427.
4 H. A. Shih, J. S. Loeffler and N. J. Tarbell, Effects of CNS Radiation Therapy, *Late Effects of Treatment for Brain Tumors*, Springer, US, 2009, p. 23.
5 S. P. Jackson and J. Bartek, *Nature*, 2009, **461**, 1071.
6 T. Helleday, E. Petermann, C. Lundin, B. Hodgson and R. A. Sharma, *Nat. Rev. Cancer*, 2008, **8**, 193.
7 S. Sharma and S. C. Raghavan, *J. Nucleic Acids*, 2010, **1**, 2010.
8 M. R. Lieber, K. Yu and S. C. Raghavan, *DNA Repair*, 2006, **5**, 1234.
9 C. Wyman and R. Kanaar, *Annu. Rev. Genet.*, 2006, **40**, 363.
10 V. Gopalakrishnan and S. C. Raghavan, *Future Oncol.*, 2012, **8**, 1121.
11 M. Nambiar and S. C. Raghavan, *Cell. Mol. Life Sci.*, 2013, 1.
12 M. Nambiar and S. C. Raghavan, *Nucleic Acids Res.*, 2011, **39**, 5813.
13 S. C. Raghavan, P. C. Swanson, X. Wu, C. L. Hsieh and M. R. Lieber, *Nature*, 2004, **428**, 88.
14 F. W. Alt, Y. Zhang, F. L. Meng, C. Guo and B. Schwer, *Cell*, 2013, **152**, 417.
15 M. L. Hefferin and A. E. Tomkinson, *DNA Repair*, 2005, **4**, 639.
16 M. Srivastava, M. Nambiar, S. Sharma, S. S. Karki, G. Goldsmith, M. Hegde, S. Kumar, M. Pandey, R. K. Singh, P. Ray, R. Natarajan, M. Kelkar, A. De, B. Choudhary and S. C. Raghavan, *Cell*, 2012, **151**, 1474.
17 J. W. Lee, E. D. Jeong, E. J. Cho, J. A. Gardella Jr, W. Hicks Jr, R. Hard and F. V. Bright, *Appl. Surf. Sci.*, 2008, **255**, 2360.
18 W. Chen, Y. Shi, H. Feng, M. Du, J. Z. Zhang, J. Hu and D. J. Yang, *J. Phys. Chem. B*, 2012, **116**, 9231.
19 D. Qiu, C. Flood and T. A. Cosgrove, *Langmuir*, 2008, **24**, 2983.
20 F. John, J. George, S. V. Vartak, M. Srivastava, P. A. Hassan, V. K. Aswal, S. S. Karki and S. C. Raghavan, *Macromol. Biosci.*, 2014, DOI: 10.1002/mabi.201400480.
21 S. Alexander, T. Cosgrove, T. C. Castle, I. Grillo and S. W. Prescott, *J. Phys. Chem. B*, 2012, **116**, 11545.
22 P. Alexandridis and L. Yang, *Macromolecules*, 2000, **33**, 5574.
23 M. J. Ansari, S. Ahmad, K. Kholi, J. Ali and R. K. Khar, *J. Pharm. Biomed. Anal.*, 2005, **39**, 132.